



Crystal structure of leukotriene A₄ hydrolase in complex with kelatorphan, implications for design of zinc metallopeptidase inhibitors [☆]

Fredrik Tholander ^{a,1}, Bernard-Pierre Roques ^c, Marie-Claude Fournié-Zaluski ^d,
Marjolein M.G.M. Thunnissen ^b, Jesper Z. Haeggström ^{a,*}

^a Department of Medical Biochemistry and Biophysics, Division of Chemistry II, Karolinska Institute, S-171 77 Stockholm, Sweden

^b Department of Molecular Biophysics, Kemistisentrum, Lund University, S-221 00 Lund, Sweden

^c Département de Pharmacochimie Moléculaire et Structurale, 4 Avenue de l'Observatoire, 75270 Paris Cedex 06, France

^d Pharmaleads, 11 rue Watt, 7513 Paris, France

ARTICLE INFO

Article history:

Received 1 June 2010

Revised 24 June 2010

Accepted 25 June 2010

Available online 6 July 2010

Edited by Christian Griesinger

Keywords:

Leukotriene

Leukotriene B₄

LTA₄ hydrolase

Amino peptidase

Cardiovascular

Inflammation

ABSTRACT

Leukotriene A₄ hydrolase (LTA₄H) is a key enzyme in the inflammatory process of mammals. It is an epoxide hydrolase and an aminopeptidase of the M1 family of the MA clan of Zn-metallopeptidases. We have solved the crystal structure of LTA₄H in complex with N-[3(R)-[(hydroxyamino)carbonyl]-2-benzyl-1-oxopropyl]-L-alanine, a potent inhibitor of several Zn-metalloenzymes, both endopeptidases and aminopeptidases. The inhibitor binds along the sequence signature for M1 aminopeptidases, GXMEN. It exhibits bidentate chelation of the catalytic zinc and binds to LTA₄H's enzymatically essential carboxylate recognition site. The structure gives clues to the binding of this inhibitor to related enzymes and thereby identifies residues of their S1' sub sites as well as strategies for design of inhibitors.

© 2010 Federation of European Biochemical Societies. Published by Elsevier B.V. All rights reserved.

1. Introduction

Leukotriene A₄ hydrolase (LTA₄H) is a bifunctional zinc metalloenzyme possessing an aminopeptidase as well as an epoxide hydrolase activity. Whereas the former activity is yet of unknown physiological relevance the latter catalyzes the formation of the potent chemotaxin leukotriene B₄ (LTB₄), a substance which is fundamental to the inflammatory response of mammals and possibly all vertebrates. Even though the immediate effect of LTB₄ is neutrophil recruitment, which is elicited already at nanomolar concentrations [1], LTB₄ is also known to modulate the immune response [2],

Abbreviations: p-NAN, para-nitroaniline; p-NA, para-nitroanilide; LTA₄, leukotriene A₄; LTA₄H, Leukotriene A₄ hydrolase; SDS-PAGE, sodium dodecyl polyacrylamide gel electrophoresis; HPLC, high performance liquid chromatography; kelatorphan, N-[3(R)-[(hydroxyamino)carbonyl]-2-benzyl-1-oxopropyl]-L-alanine

[☆] Atomic coordinates and structure factors are available at the Protein Data Bank (<http://www.rcsb.org/>) with PDBID 3B7U.

* Corresponding author. Fax: +46 8 7360439.

E-mail addresses: fredrik.tholander@molbio.su.se (F. Tholander), jesper.haeggstrom@ki.se (J.Z. Haeggström).

¹ Present address: Department of Molecular Biology and Functional Genomics, Stockholm University, 106 91 Stockholm, Sweden.

to participate in the host-defense against infection [3], to regulate lipid metabolism [4] and to be a key-mediator of the lethal effect of PAF-induced systemic shock [5,6]. Elevated levels of LTB₄ have been detected in afflicted tissues of several inflammatory diseases, e.g., rheumatoid arthritis [7], inflammatory bowel disease [8] and psoriasis [9]. It has recently been demonstrated that LTA₄H is upregulated in atherosclerotic plaques of humans thus suggesting a role for LTB₄ in cardiovascular disease [10]. Furthermore, recent reports have shown that LTB₄ also mediates recruitment of certain T-cells to the site of inflammation, thereby identifying LTB₄ as a link between the innate and adaptive immune response [11–13].

Since LTB₄ is undoubtedly of pathological relevance it is particularly interesting to control its biosynthesis as a means to treat different inflammatory disorders. To this end, the development and analysis of efficient inhibitors targeted against LTA₄H is highly interesting. Here we report the crystal structure of LTA₄H in complex with N-[3(R)-[(hydroxyamino)carbonyl]-2-benzyl-1-oxopropyl]-L-alanine (kelatorphan), a di-peptide related substance in which the α-amino group has been replaced by a bidentate metal-chelating hydroxamic acid moiety.

Kelatorphan was originally designed to inhibit the endopeptidase neprilysin (K_i 2 nM) but was subsequently found to be potent

also towards human aminopeptidase N (APN) (K_i 0.7 μM) and LTA4H (K_i of 5 nM), even though it does not contain the free amino group typically required for recognition by aminopeptidases [14–16]. Here we report the crystal structure of LTA4H in complex with kelatorphan, which reveals a binding arrangement relying on a conserved sequence motif (GXMEN of M1 aminopeptidases), strong zinc chelation and binding to LTA4H's carboxylate recognition site. Since binding of kelatorphan relies on conserved structural elements it is possible to extrapolate our findings to other homologous Zn metallo enzymes.

2. Materials and methods

2.1. Materials

Leukotriene A₄ (LTA₄) methyl ester was purchased from BIOMOL Res. Lab, Plymouth Meeting, PA, USA and saponified in tetrahydrofuran with 1 M LiOH (6% v/v) for 48 h at 4 °C. Bradford protein dye-reagent was from Bio-Rad (Bio-Rad Laboratories AB, Sweden) and other chemicals were from Sigma (Sigma-Aldrich Sweden AB, Sweden). Kelatorphan was synthesized as described [17,18].

2.2. Protein expression and purification

Expression of (His)₆-tagged protein in *Escherichia coli* and subsequent purification with Ni-affinity chromatography followed by anion exchange chromatography was performed as previously described [16,19]. The final anion exchange step was only performed on protein preparations used for crystallization. The protein purity was assessed by sodium dodecyl polyacrylamide gel electrophoresis (SDS-PAGE) using 10–15% gradient gels on a Pharmacia phast system. Protein concentration was determined according to the Bradford method using bovine serum albumin as standard. To verify the functional integrity of the protein, the tri-peptidase activity was confirmed with a recently described novel methodology utilizing competing substrates [20].

2.3. Aminopeptidase inhibition assays

Five sets of initial velocity measurements were performed. Within a set, substrate concentration was varied while concentration of inhibitor was kept constant. Inhibitor concentration was varied between sets. The complete experiment was repeated 3 times.

Aliquots (50 μl) of equilibrated solutions containing 1 μg protein, 500 mM KCl, 250 mM Tris-HCl pH 7.5 and various amounts of inhibitor were added to the wells of a microtiter plate. Reactions were initiated by the addition of 200 μl of ala-*p*-NA of various concentrations. The amount of *para*-nitroaniline (*p*-NAn) formation was monitored for 15 min in a MCC/340 multiscan spectrophotometer as increase in absorbance at 405 nm. To correct for spontaneous hydrolysis of ala-*p*-NA, absorbance of incubations without enzyme was subtracted. A molar response factor of 8065 M⁻¹ was used for *p*-NAn.

2.4. Epoxide hydrolase inhibition assay

Three sets of dose-response measurements with constant substrate concentration and varied inhibitor concentration were performed. Aliquots (100 μl) of 50 mM Tris-HCl pH 8.0 containing 2.5 μg of protein and various amounts of inhibitor were incubated for 20 min on ice. Reactions were initiated by addition of 1 μl LTA₄ (final concentration 150 μM) and stopped after 15 s with 200 μl of methanol, containing PGB₂ as internal standard. Samples were subsequently diluted with 1 ml water and acidified with 10 μl of

acetic acid (10%). Metabolites were isolated by solid phase extraction on Chromabond C18 columns. Samples were loaded on the columns and washed with 1 ml 25% methanol followed by extraction with 250 μl 100% methanol. Extracted samples were diluted with 250 μl water and subsequently analyzed by high performance liquid chromatography with a Waters Nova-Pak C18 column and isocratic elution with methanol/acetonitrile/water/acetic acid (30:30:40:0.01 by volume) at a flow rate of 1.2 ml/min. Metabolites were detected by their UV absorbance at 270 nm and quantified using Chromatography Station for Windows version 1.7 computer software. Calculations were based on peak area measurements and the known extinction coefficients for the internal standard PGB₂ (30 000 M⁻¹ × cm⁻¹) as well as LTB₄ (50 000 M⁻¹ × cm⁻¹).

2.5. Determination of kinetic parameters

Data obtained from the aminopeptidase inhibition assay was analyzed using the Dynafit program [21]. The program numerically fits various models for inhibition to the data and performs model discrimination analysis. K_i values from the model obtaining the highest statistical significance are reported and standard errors are the ones calculated by the software.

For determination of IC₅₀ values, a standard four parameter Hill equation (with parameters for top and bottom plateaus set to constant values) was fitted to the data and the model-to-data fit analyzed using the Solverstat software [22].

2.6. Crystallization

Crystals of LTA4H complexed with kelatorphan were obtained by co-crystallization of enzyme and inhibitor using the liquid-liquid diffusion method described previously [19]. Briefly, 5 μl of precipitation solution (28% (v/v) PEG8000, 50 mM sodium acetate, 0.1 M imidazole buffer, pH 6.8, and 5 mM YbCl₃), was injected into the bottom of a melting point capillary and an equal volume of LTA4H (5 mg/ml) in 10 mM Tris-HCl, pH 7.5, containing 1 mM kelatorphan, was layered on top.

2.7. Diffraction data collection

For data collection, crystals were soaked in 14% (w/v) PEG8000, 25 mM sodium acetate, 50 mM imidazole buffer, pH 6.8, 2.5 mM YbCl₃ and 25% (v/v) glycerol. Data was collected at the beamline I711 of Max-Lab, Lund, Sweden. During data collection the crystal was kept under a stream of liquid nitrogen. A complete set of data was collected from one single crystal.

2.8. Data processing and refinement

Diffraction data were processed with Mosflm [23] and programs of the CCP4 program suit [24]. As a starting model for the refinement the crystal structure of [E271Q]LTA4H was used (PDB ID 1H19). Prior to initial refinement all solvent and ligand atoms, except the active site Zn ion were removed, and all B-factors set to 15. The same set of reflections (mounting to 3.3% of the data set) as in the starting model was set aside for the R_{free} calculations. Refinement was performed according to the maximum likelihood principle using remlcp software [25]. In the initial rounds of refinement the protein was treated as a rigid body followed by a restrained refinement including isotropic B-factors. Manual model building and interpretation of electron density maps was then performed with the XtalView program [26]. While monitoring the R values, additional rounds of automatic building of solvent atoms and restrained refinement interspersed with manual model building was then performed until the structures converged. Figures were

generated with Vida (OpenEye Scientific Software, Inc.) and SwissPDB Viewer (<http://www.expasy.org/spdbv/>).

3. Results and discussion

3.1. Protein expression and purification

From 4.5 l of cell culture approximately 10 mg of recombinant protein was obtained. After purification, LTA4H appeared as a single band on an SDS–PAGE gel. Protein concentration was determined and adjusted to approximately 5.0 mg/ml.

3.2. Enzyme inhibition assays

For the peptidase activity K_i was determined to 9.0 ± 2.5 nM, in agreement with a previous report [14]. For the epoxide hydrolase activity IC_{50} was determined to 170 ± 30 nM (corresponding to a K_i of 11 nM at the given assay conditions). Thus, both assays gave similar results for the inhibitory potency of kelatorphan. An attempt to test the inhibitor potency in a whole cell assay was also made, but the effect of the inhibitor was weak and an accurate IC_{50} value could not be determined ($IC_{50} \gg 10 \mu\text{M}$), in agreement with a previous report [14]. The high polarity of kelatorphan ($\log P = 0.2$, $\log D @ \text{pH} 7.4 = -3.37$) prevents it from entering the cell interior and explains its weak effect in the whole cell assay.

3.3. Crystallization, X-ray data collection and structure refinement

Plate-like crystals were obtained by the liquid–liquid diffusion method and appeared within two to three weeks after set up. Data collection statistics, cell parameters and space groups are given in Table 1.

3.4. Model building

The final refined model is of good quality with well-defined electron density for all residues except for a few residues in the N- and C-termini. Electron density for the inhibitor was clearly visible in the initial $F_o - F_c$ difference map of the starting model and the inhibitor could be modeled unambiguously with full occupancy with B-factors in the same range as the surrounding protein atoms (Fig. S1). For additional refinement statistics and model quality data see Table 1.

3.5. Crystal structure of kelatorphan in complex with LTA4H

Kelatorphan binds in an extended beta-sheet conformation between the zinc ion and Arg-563 (Fig. 1). The carboxyl moiety forms two hydrogen bonds with Arg-563, and the hydroxamate moiety chelates the zinc ion in a bidentate fashion. Due to chemical similarities, the binding mode of kelatorphan is interesting to compare with those of tri-peptide substrates (Arg–Ser–Arg and Arg–Ala–Arg, PDB IDs 3B7S and 3B7T) and phosphinic acid inhibitors (RB3040 and RB3041, PDB IDs 3B7R and 2R59), described previously [27]. Thus, the interaction between the carboxy terminus of kelatorphan and the enzyme is identical with the corresponding interactions for substrates and transition state analogues. The zinc chelation is slightly asymmetric with coordinate bond distances of 2.1 and 2.3 Å for the zinc–carbonyl oxygen and the zinc–hydroxyl oxygen, respectively. This results in a slightly distorted square based pyramidal total coordination geometry of the zinc ion.

The phenylalanine moiety of kelatorphan occupies the same position as the corresponding P1' side-chain of the RB3040 and RB3041 inhibitors. However, in one of these structures (LTA4H–RB3041) the plane of the phenyl ring of the inhibitor is rotated by approximately 90° with respect to the corresponding ring

Table 1

Data collection and refinement statistics. Values for the highest resolution shell are given in parenthesis.

Kelatorphan-LTA4H	
<i>Data collection statistics</i>	
Resolution range (Å)	15–1.9
λ (Å)	1.089
R_{merge}^a (%)	8.7 (25)
Completeness (%)	97.5 (96)
No. of unique reflections	52 364
Mean I/σ	9.8 (2.9)
Multiplicity of observation	3.5 (2.5)
Cell dimensions (Å)	$a = 77.83$; $b = 87.14$; $c = 99.19$
Cell dimension ($^\circ$)	$\alpha = \beta = \gamma = 90^\circ$
Space group	P212121
<i>Refinement</i>	
Resolution range (Å)	14.65–1.9
R_{factor}^b	17.0
R_{free}^c	21.7
Rmsd of bond length (Å)	0.021
Rmsd of bond angle ($^\circ$)	1.77
Average B main chain (Å^2)	11.4
Average B side chain (Å^2)	14.6
Average B waters (Å^2)	19.8
Average B inhibitor (Å^2)	15
Ramachandran d (%)	7.2, 0.4, 0
No. of water molecules	420
Other non-protein residues	Zn $^{2+}$, Yb $^{3+}$, acetate, kelatorphan, imidazole

^a $R_{\text{merge}} = \sum_j \sum_h |I_{hj} - I_h| / \sum_j \sum_h I_{hj}$ - where I_{hj} is the j th observation of reflection h and I_h is the weighted mean of all measurements of h .

^b $R_{\text{factor}} = \sum_j |F_{\text{obs}} - F_{\text{calc}}| / \sum_j |F_{\text{obs}}|$ - where F_{obs} and F_{calc} are the observed and calculated structure factor amplitudes, respectively.

^c R_{free} is the R_{factor} calculated for the test set of reflections (3.3%), which are omitted during the refinement process.

^d Fraction of non-glycine residues in additionally allowed, generously allowed and disallowed regions of the Ramachandran plot.

of the other complexes (indicated with a curved arrow in the lower panels of Fig. 1). The methyl moiety of kelatorphan, which is equivalent to a P2' alanine residue, binds at a position corresponding to the P2' phenyl group of RB3041 or arginyl side chains of the tri-peptide substrates. Because the sub-pocket here is large, the methyl moiety of kelatorphan does not form any clear interactions with the enzyme.

Interestingly, kelatorphan and the phosphinic acid inhibitors (RB3040 and RB3041) exhibit similar inhibition potencies towards LTA4H suggesting that the sum of the stabilizing interactions are similar in the different complexes. Consistent with this assumption, the structural data show that metal binding (penta-valent zinc coordination geometry), binding along the conserved GXMEN motif and carboxylate binding by Arg-563 are very similar in the structures and thus constitute the main determinants for inhibition potency. The small differences in binding affinities are explained by the different side-chains.

In the overall structure, kelatorphan does not induce any significant structural changes compared to previously analyzed inhibitors. For instance, compared to the LTA4H–RB3041 structure, the root mean square deviation between all backbone atoms is 0.23 Å. In the active site, the only residue that has adopted a significantly different conformation is Gln-136, which exhibits a 90° difference in its $C\gamma$ – $C\delta$ dihedral between the two structures. This torsional twist is induced by the differing P1 residue: while kelatorphan lacks such a side chain RB3041 possesses a P1 phenylalanine moiety.

3.6. Binding of kelatorphan to other aminopeptidases

In addition to LTA4H and human APN, kelatorphan also inhibits other aminopeptidases of the M1 family [18,28]. We here present the first example of a structure of this compound bound to its

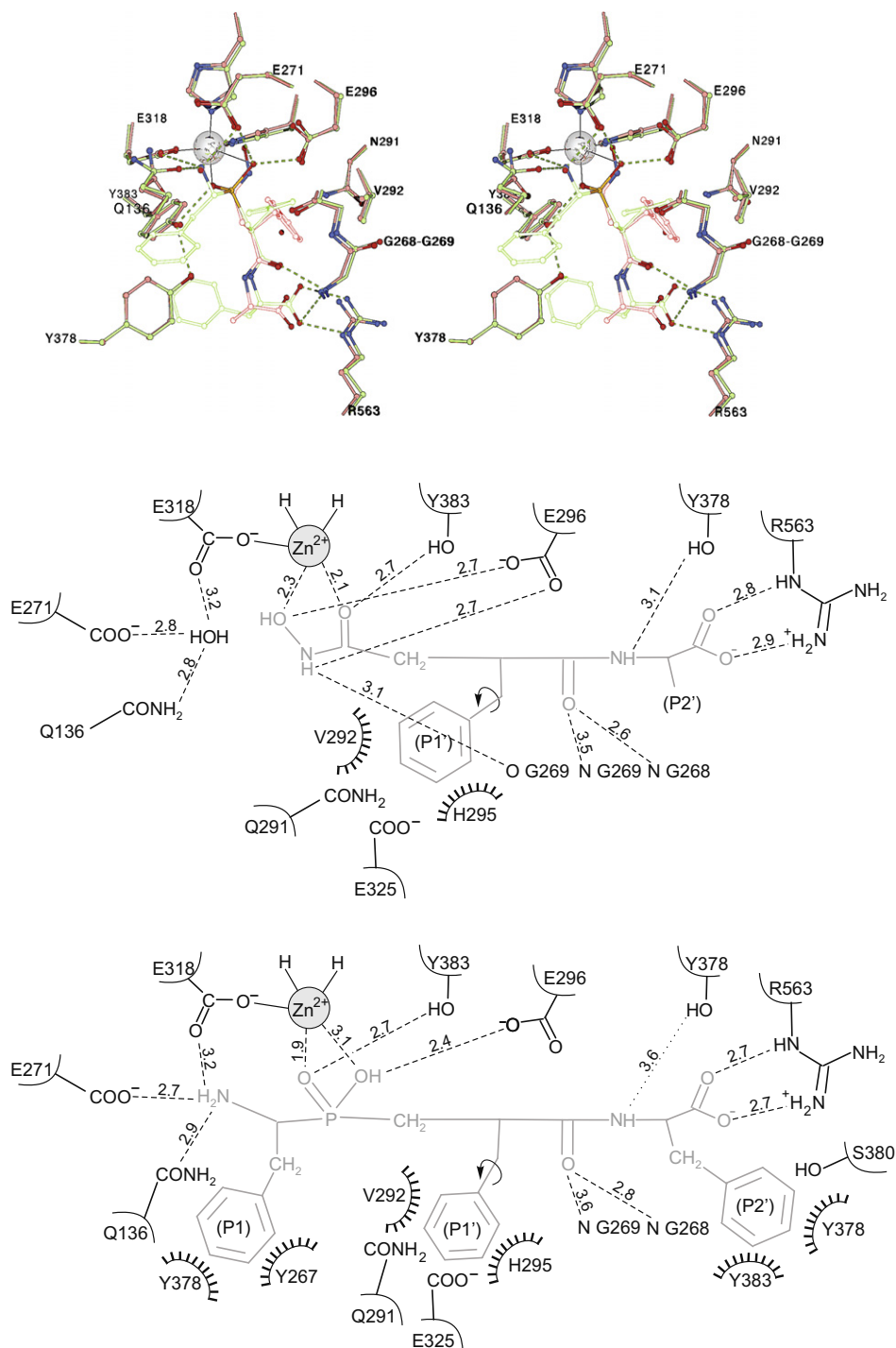


Fig. 1. Binding of kelatorphan to LTA4H and comparison to RB3041. Top panel: stereo representation of kelatorphan and selected key residues. For comparison, the structure is superimposed onto a previously solved structure of LTA4H complexed with the phosphinic acid inhibitor RB3041 [27]. Carbon atoms of the LTA4H-kelatorphan structure are shown in pink and of the LTA4H-RB3041 structure in green, the zinc ion is shown as a metallic sphere. Middle panel: A schematic description highlighting important interactions in the binding of kelatorphan by LTA4H. Lower panel: schematic representation of the binding of RB3041 to LTA4H. The protein is shown in black and the bound inhibitors in gray, selected non-bonding interactions are presented with dotted lines (middle and lower panels). The curved arrow indicates a torsional difference between kelatorphan and RB3041 (middle and lower panels).

target enzyme. The structure may serve as a template for the binding mode of this inhibitor to other members of the M1 family of aminopeptidases. The basic binding mode of the inhibitor is probably very similar between different enzymes, since both the zinc site and the GXMEN sequence motif are conserved among members of the M1 family and essential for substrate and inhibitor binding [15,16,27,29–32].

In LTA4H the carboxyl moiety of tri-peptide substrates (the preferred substrate of LTA4H) binds to Arg-563, a functionality which is absent in several other aminopeptidases adopted to bind longer peptides. This is reflected by the fact that kelatorphan is a significantly weaker inhibitor of human APN, which lacks such a residue, as compared to LTA4H. Thus, even though kelatorphan is likely to be active against several other M1 aminopeptidases, its potency

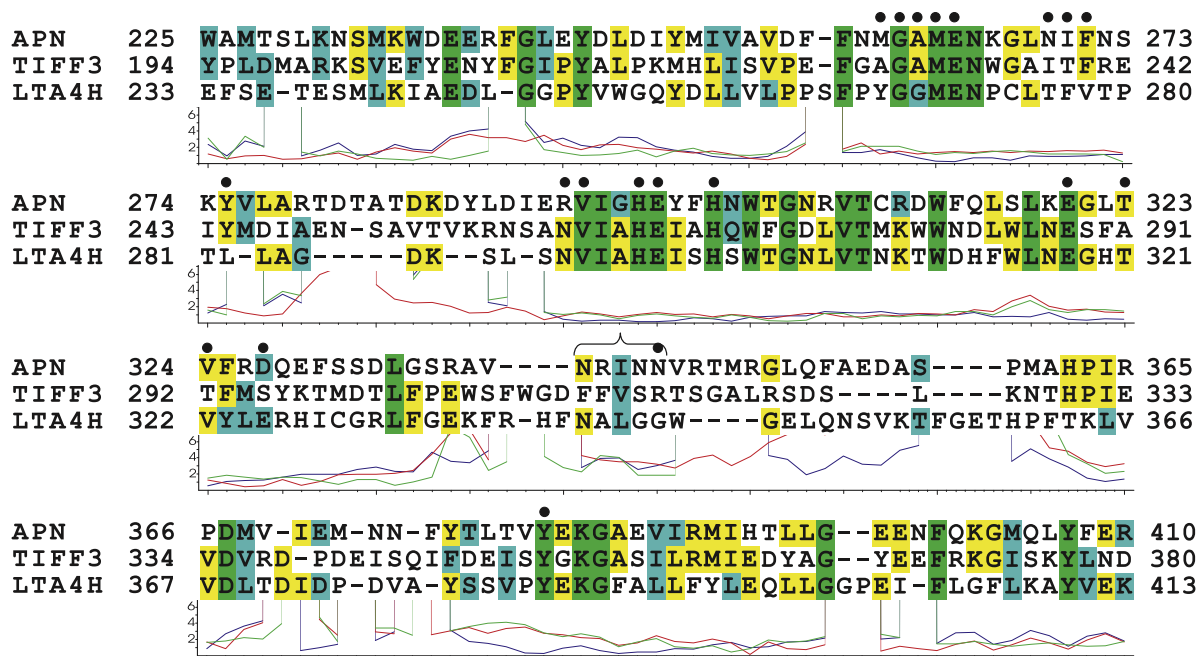


Fig. 2. Structurally corrected sequence alignment of APN, the tricorner interacting factor F3 and LTA4H. Subsequences corresponding to ~200 residues of the central catalytic domain of LTA4H that were used in the alignment are shown. Conserved residues are shaded in green, identical residues in yellow and similar residues in cyan. Positions marked with a black dot indicate residues in APN or TIFF3 that are within interacting distance of the phenylalanine side chain of kelatorphan and thereby define potential residues of the S1' sub-pocket, see Section 3.6 for details. Underneath each block of sequences, a diagram indicates the Euclidian distance between corresponding α -carbons of each structure. Green trace, LTA4H-TIFF3; blue trace LTA4H-APN; red trace, APN-TIFF3. The sequence alignment was adjusted according to the relative positioning of the superimposed structures. Brackets () mark residues that exhibit poor matching between α -carbon positions where the choice of corresponding residues are ambiguous.

may partly depend on the presence of an anchoring site for its carboxyl moiety.

Besides LTA4H, one archaic, two prokaryotic, and one eukaryotic aminopeptidase of the M1 family of metalloproteases have been structurally determined; the tri-tricorn interacting factor F3 from (TIFF3) *Thermoplasma acidophilum* and APN from *E. coli* and *Colwellia psychrerythraea*, and APN from *Plasmodium falciparum* [19,33–37]. Superimposing e.g., LTA4H-APN (*E. coli*), APN-TIFF3, and LTA4H-TIFF3 gives root mean square deviations of 1.4 Å for 325 equivalent C- α atoms for LTA4H-APN, 1.8 Å for 281 C- α atoms of APN-TIFF3, and 1.7 Å for 244 C- α atoms of TIFF3-LTA4H. Significant parts of the structural elements surrounding the active site align very well in space (Fig. 2); conclusions regarding functional conservation of such regions are likely to be reliable.

Since the phenylalanine moiety of kelatorphan corresponds to the P1' residue of peptide substrates, the S1' sub site and surrounding residues of these enzymes can be identified (Fig. 2). To identify these residues, the torsions of the P1' phenylalanine moiety of kelatorphan were scanned. Residues of the structures superimposed onto LTA4H, which came close to the P1' side chain, was then flagged as potential S1' residues (Fig. 2). This allowed a generous definition of the S1' sub site. The cutoff criteria for an interacting residue was strictly distance based (4 Å), for instance stereochemical or energetic effects were not taken into account.

Notably, most identified residues are located in parts of the structures that align well in three dimensions, as indicated in Fig. 2. Extrapolation of the functional role of a particular residue of LTA4H to other aminopeptidases are more reliable for residues found in such well-aligned regions, e.g. as seen for the identified residues of the S1' sub-pocket (Fig. 2). Sequence alignments would allow simple identification of these residues in yet other M1 aminopeptidases. To experimentally verify their potential role in substrate specificity, future mutational studies may be utilized.

In conclusion, the LTA4H-kelatorphan crystal structure reveals that the binding of the inhibitor partly relies on conserved struc-

tural elements (the catalytic zinc site and the GXMEN motif of M1 aminopeptidases) as well as elements unique for LTA4H. Therefore, it becomes possible to extrapolate our findings regarding kelatorphan binding and specificity to other homologous zinc metalloenzymes, which in turn may aid in development of isozyme selective inhibitors that can discriminate between LTA4H and other zinc aminopeptidases.

Acknowledgements

The authors thank Eva Ohlson for technical assistance and the personnel at the I711 beam-line of the MAX-Lab synchrotron facility for assistance with data collection. The work was funded by The Swedish Research Council (10350, 20854, and Linneus Grant CERIC), CIDaT (Vinnova), and EC FP6 and FP7 funding (005033, 201668). Disclaimer: The report reflects only the author's views and the European Commission is not liable for any use that may be made of the information herein.

Appendix A. Supplementary data

Supplementary data associated with this article can be found, in the online version, at doi:10.1016/j.febslet.2010.06.044.

References

- [1] Samuelsson, B. (1983) Leukotrienes: mediators of immediate hypersensitivity reactions and inflammation. *Science* 220, 568–575.
- [2] Griffiths, R.J. et al. (1997) Collagen-induced arthritis is reduced in 5-lipoxygenase-activating protein-deficient mice. *J. Exp. Med.* 185, 1123–1129.
- [3] Baillie, M.B., Standiford, T.J., Laichalk, L.L., Coffey, M.J., Strieter, R. and Peters-Golden, M. (1996) Leukotriene-deficient mice manifest enhanced lethality from *Klebsiella pneumoniae* in association with decreased alveolar macrophage phagocytic and bactericidal activities. *J. Immunol.* 157, 5221–5224.
- [4] Devchand, P.R., Keller, H., Peters, J.M., Vazquez, M., Gonzalez, F.J. and Wahli, W. (1996) The PPAR α -leukotriene B4 pathway to inflammation control. *Nature* 384, 39–43.

- [5] Chen, X.-S., Sheller, J.R., Johnson, E.N. and Funk, C.D. (1994) Role of leukotrienes revealed by targeted disruption of the 5-lipoxygenase gene. *Nature* 372, 179–182.
- [6] Byrum, R.S., Goulet, J.L., Snouwaert, J.N., Griffiths, R.J. and Koller, B.H. (1999) Determination of the contribution of cysteinyl leukotrienes and leukotriene B4 in acute inflammatory responses using 5-lipoxygenase- and leukotriene A4 hydrolase-deficient mice. *J. Immunol.* 163, 6810–6819.
- [7] Davidson, E.M., Rae, S.A. and Smith, M.J.H. (1982) Leukotriene B4 in synovial fluid. *J. Pharm. Pharmacol.* 34, 410.
- [8] Lobos, E.A., Sharon, P. and Stenson, W.F. (1987) Chemotactic activity in inflammatory bowel disease: role of leukotriene B4. *Dig. Dis. Sci.* 32, 1380–1388.
- [9] Brain, S.D., Camp, R.D., Cunningham, F.M., Dowd, P.M., Greaves, M.W. and Black, A.K. (1984) Leukotriene B4-like material in scale of psoriatic skin lesions. *Br. J. Pharmacol.* 83, 313–317.
- [10] Qiu, H. et al. (2006) Expression of 5-lipoxygenase and leukotriene A4 hydrolase in human atherosclerotic lesions correlates with symptoms of plaque instability. *Proc. Natl. Acad. Sci. USA* 103, 8161–8166.
- [11] Ott, V.L., Cambier, J.C., Kappler, J., Marrack, P. and Swanson, B.J. (2003) Mast cell-dependent migration of effector CD8+ T cells through production of leukotriene B4. *Nat. Immunol.* 4, 974–981.
- [12] Tager, A.M. et al. (2003) Leukotriene B4 receptor BLT1 mediates early effector T cell recruitment. *Nat. Immunol.* 4, 982–990.
- [13] Goodarzi, K., Goodarzi, M., Tager, A.M., Luster, A.D. and von Andrian, U.H. (2003) Leukotriene B4 and BLT1 control cytotoxic effector T cell recruitment to inflamed tissues. *Nat. Immunol.* 4, 965–973.
- [14] Penning, T.D., Askonas, L.J., Djuric, S.W., Haack, R.A., Yu, S.S., Michener, M.L., Krivi, G.G. and Pyla, E.Y. (1995) Kelatorphan and related analogs – potent and selective inhibitors of leukotriene A4 hydrolase. *Bioorg. Med. Chem. Lett.* 5, 2517–2522.
- [15] Luciani, N., Marie-Claire, C., Ruffet, E., Beaumont, A., Roques, B.P. and Fournie-Zaluski, M.C. (1998) Characterization of Glu350 as a critical residue involved in the N-terminal amine binding site of aminopeptidase N (EC 3.4.11.2): insights into its mechanism of action. *Biochemistry* 37, 686–692.
- [16] Rudberg, P.C., Tholander, F., Thunnissen, M.G.M. and Haeggström, J.Z. (2002) Leukotriene A4 hydrolase/aminopeptidase: glutamate 271 is a catalytic residue with specific roles in two distinct enzyme mechanisms. *J. Biol. Chem.* 277, 1398–1404.
- [17] Fournie-Zaluski, M.C., Chaillet, P., Bouboutou, R., Coulaud, A., Cherot, P., Waksman, G., Costentin, J. and Roques, B.P. (1984) Analgesic effects of kelatorphan, a new highly potent inhibitor of multiple enkephalin degrading enzymes. *Eur. J. Pharmacol.* 102, 525–528.
- [18] Fournie-Zaluski, M.C., Coulaud, A., Bouboutou, R., Chaillet, P., Devin, J., Waksman, G., Costentin, J. and Roques, B.P. (1985) New bidentates as full inhibitors of enkephalin-degrading enzymes: synthesis and analgesic properties. *J. Med. Chem.* 28, 1158–1169.
- [19] Thunnissen, M.G.M., Nordlund, P. and Haeggström, J.Z. (2001) Crystal structure of human leukotriene A4 hydrolase, a bifunctional enzyme in inflammation. *Nat. Struct. Biol.* 8, 131–135.
- [20] Tholander, F. and Haeggstrom, J.Z. (2007) Assay for rapid analysis of the tripeptidase activity of LTA4 hydrolase. *Proteins* 67, 1113–1118.
- [21] Kuzmic, P. (1996) Program DYNAFIT for the analysis of enzyme kinetic data: application to HIV proteinase. *Anal. Biochem.* 237, 260–273.
- [22] Comuzzi, C., Polese, P., Melchior, A., Portanova, R. and Tolazzi, M. (2003) SOLVERSTAT: a new utility for multipurpose analysis. An application to the investigation of dioxygenated Co(II) complex formation in dimethylsulfoxide solution. *Talanta*, 67–80.
- [23] Leslie, A. G. W. (1992) Recent changes to the MOSFLM package for processing film and image plate data. In Joint CCP4 and ESF-EACMB Newsletter on Protein Crystallography No. 26, Laboratory, D. (Eds.), Warrington, UK.
- [24] Collaborative Computing Project Number 4. (1994) The CCP4 suite: programs for protein crystallography. *Acta Crystallogr., Sect. D: Biol. Crystallogr.*, 50, 760–763.
- [25] Murshudov, G.N., Vagin, A.A. and Dodson, E.J. (1997) Refinement of macromolecular structures by the maximum-likelihood method. *Acta Crystallogr., Sect. D: Biol. Crystallogr.* D53, 240–255.
- [26] McRee, D.E. (1999) XtalView/Xfit – A versatile program for manipulating atomic coordinates and electron density. *J. Struct. Biol.* 125, 156–165.
- [27] Tholander, F., Muroya, A., Roques, B.P., Fournie-Zaluski, M.C., Thunnissen, M.M. and Haeggstrom, J.Z. (2008) Structure-based dissection of the active site chemistry of leukotriene A4 hydrolase: implications for M1 aminopeptidases and inhibitor design. *Chem. Biol.* 15, 920–929.
- [28] Bouboutou, R., Waksman, G., Devin, J., Fournie-Zaluski, M.C. and Roques, B.P. (1984) Bidentate peptides: highly potent new inhibitors of enkephalin degrading enzymes. *Life Sci.* 35, 1023–1030.
- [29] Medina, J.F., Wetterholm, A., Rådmark, O., Shapiro, R., Haeggström, J.Z., Vallee, B.L. and Samuelsson, B. (1991) Leukotriene A4 hydrolase: determination of the three zinc-binding ligands by site-directed mutagenesis and zinc analysis. *Proc. Natl. Acad. Sci. USA* 88, 7620–7624.
- [30] Wetterholm, A., Medina, J.F., Rådmark, O., Shapiro, R., Haeggström, J.Z., Vallee, B.L. and Samuelsson, B. (1991) Recombinant mouse leukotriene A4 hydrolase: a zinc metalloenzyme with dual enzymatic activities. *Biochim. Biophys. Acta* 1080, 96–102.
- [31] Iturrioz, X., Rozenfeld, R., Michaud, A., Corvol, P. and Llorens-Cortes, C. (2001) Study of asparagine 353 in aminopeptidase A: characterization of a novel motif (GXMEN) implicated in exopeptidase specificity of monozinc aminopeptidases. *Biochemistry* 40, 14440–14448.
- [32] Vazeux, G., Iturrioz, X., Corvol, P. and Llorens-Cortes, C. (1998) A glutamate residue contributes to the exopeptidase specificity in aminopeptidase A. *Biochem. J.* 334, 407–413.
- [33] Kyrieleis, O.J., Goettig, P., Kiefersauer, R., Huber, R. and Brandstetter, H. (2005) Crystal structures of the tricorn interacting factor F3 from *Thermoplasma acidophilum*, a zinc aminopeptidase in three different conformations. *J. Mol. Biol.* 349, 787–800.
- [34] Addlagatta, A., Gay, L. and Matthews, B.W. (2006) Structure of aminopeptidase N from *Escherichia coli* suggests a compartmentalized, gated active site. *Proc. Natl. Acad. Sci. USA* 103, 13339–13344.
- [35] Ito, K., Nakajima, Y., Onohara, Y., Takeo, M., Nakashima, K., Matsubara, F., Ito, T. and Yoshimoto, T. (2006) Crystal structure of aminopeptidase N (proteobacteria alanyl aminopeptidase) from *Escherichia coli* and conformational change of methionine 260 involved in substrate recognition. *J. Biol. Chem.* 281, 33664–33676.
- [36] McGowan, S. et al. (2009) Structural basis for the inhibition of the essential *Plasmodium falciparum* M1 neutral aminopeptidase. *Proc. Natl. Acad. Sci. USA* 106, 2537–2542.
- [37] Bauvois, C., Jacquamet, L., Huston, A.L., Borel, F., Feller, G. and Ferrer, J.L. (2008) Crystal structure of the cold-active aminopeptidase from *Colwellia psycherythraea*, a close structural homologue of the human bifunctional leukotriene A4 hydrolase. *J. Biol. Chem.* 283, 23315–23325.